Article

Not peer-reviewed version

The Light Wavelength, Intensity, and Biasing Voltage Dependency of Dark and Photocurrent Density of Solution-Processed P3HT:PC61BM Photodetector for Sensing Application

Farjana Akter Jhuma , Kentaro Harada , Muhamad Affiq Bin Misran , Hin-Wai Mo , Hiroshi Fujimoto , Reiji Hattori *

Posted Date: 8 August 2024

doi: 10.20944/preprints202408.0609.v1

Keywords: Organic photodetector; LED; photocurrent density; dark current density; on-off ratio

Article

The Light Wavelength, Intensity, and Biasing Voltage Dependency of Dark and Photocurrent Density of Solution-Processed P3HT:$PC_{61}BM$ Photodetector for Sensing Application

Farjana Akter Jhuma [1], Kentaro Harada [2], Muhamad Affiq Bin Misran [1], Hin-Wai Mo [2], Hiroshi Fujimoto [2] and Reiji Hattori [1,*]

[1] Major of Device Science and Engineering, Interdisciplinary Graduate School of Engineering Sciences, Kyushu University, Japan, jhuma.farjana.akter.233@s.kyushu-u.ac.jp
[2] OPERA Solutions Inc., 5-5 Kyudai-shimmachi, Nishi-ku, Fukuoka, 8190388 Japan, harada@opera-solutions.com
* Correspondence: hattoti.reiji.082@m.kyushu-u.ac.jp

Abstract: The promising possibility of organic photodetector (OPD) is emerging in the field of sensing applications for its tunable absorption range, flexibility, and large-scale fabrication abilities. In this work, we fabricated bulk heterojunction OPD with a device structure of glass/ITO/PEDOT:PSS/ P3HT:$PC_{61}BM$/Al by spin coating process and characterized the dark and photocurrent at different applied bias conditions for red, green, and blue incident LED light. OPD photocurrent density exhibited up to 2.5–3 orders higher magnitude compared to the dark current density at -1 V bias while it increased up to 3–4 orders at zero bias conditions for red, green, and blue lights showing an increasing trend higher voltage applied in the negative direction. Different OPD inner periphery shapes, OPD to LED distance, and OPD area were also considered to bring the variation in OPD dark and photocurrent, which can affect the on/off ratio of the OPD–LED hybrid system and is a critical phenomenon for any sensing application.

Keywords: organic photodetector; LED; photocurrent density; dark current density; on-off ratio

1. Introduction

Photodetectors are sensing devices that convert incident light to corresponding electrical signals. Organic-based photodetectors (OPDs) have attracted researchers immensely during the past decade for their enormous potential such as material tunability, low-cost solution-processability, mechanical flexibility, stretchability, lightweight, and applicability to large-area displays. These advantages have made OPDs versatile in combination with conventional photodetectors with inorganic materials [1-5]. The ability of broadband and narrowband detection has allowed OPDs to be used in optical sensing and imaging, health monitoring, artificial vision, and photonic communication [6-9]. Lee *et. al.* demonstrated an all-day-wearable health monitoring system based on a broadband OPD [10]. High-resolution image sensors with ultra-high flexibility have also been demonstrated using an OPD (Zalar *et. al.*) [11].

Generally, the response spectral range of OPD depends on photon harvesting in the organic active layer material. OPDs made out of the combination of semiconducting polymers (electron donors) and buckminsterfullerene derivatives (electron acceptors) have been proven to be capable of high detectivity and fast temporal response by many researchers [12-14]. The bulk heterojunction of an OPD, prepared from the electron donor and acceptor composite undergoes several processes like photon absorption, generation of charge-transfer (CT) excitons, and dissociation of excitons before transporting and collecting the charge carriers under light illumination. The magnitude of the photocurrent density (J_{ph}) induced by these processes depends highly on the intensity of the incident light [15]. Although the bulk heterojunction OPD suffers from a low response speed and high dark

 doi:10.20944/preprints202408.0609.v1

current issues the photocurrent can be increased by minimizing the recombination loss [16]. For any kind of sensing application, the OPD must possess the combination of a low dark current and a high photocurrent along with a high on-off ratio for achieving an excellent photo response in reverse bias conditions.

In this paper, we demonstrated the fabrication and realization of poly(3-hexylthiophene-2,5-diyl)) (P3HT): [6,6]-phenyl C_{61}-butyric acid methylester ($PC_{61}BM$) bulk heterojunction OPDs using the easy and cost-effective solution process. The OPD performances such as dark and photocurrent densities at different illumination conditions were characterized. The effect of various designs and areas of OPD was also considered to optimize the device structure for future use in sensing applications.

2. Device Fabrication and Characterization

Commercially available indium-tin-oxide (ITO) coated glass substrates were precleaned and subjected to a photolithography process, followed by wet etching for the patterning of the transparent ITO-electrode. The patterned ITO -substrates were then cleaned in an ultrasonic bath of DI water, detergent solution, acetone, and isopropyl alcohol (IPA) several times for 5 min each sequentially. The cleaned substrates were then subjected to UV/ozone treatment for 20 minutes to remove any remaining organic residues from the substrate. As the hole transport layer, the filtered poly(3,4-ethylenedioxythiophene)-poly(styrene sulfonate) (PEDOT:PSS) (Clevious P VP AI 4083, Ossila Limited, UK) solution was spin-coated on the patterned ITO substrate at 3000 rpm for 60 sec and baked at 200^{o}C for 10 min in the air. The P3HT (FUJIFILM Wako Chemicals, Japan) and $PC_{61}BM$ (Sigma Aldrich, USA) blend were used as the bulk heterojunction active layer of the OPD. Both materials were dissolved in Chlorobenzene in a 1.8:1 ratio and the prepared solution was kept on magnetic stirring for 2 days before the deposition. The P3HT:$PC_{61}BM$ solution was deposited over the PEDOT:PSS in a spin coating process at 1000 rpm speed for 50 sec followed by a baking of 80^{o}C for 5 min in an N_2 environment. Subsequently, a 100 nm Al cathode was deposited over the active layer through a metal mask in the vacuum thermal evaporation process and then annealed at 150^{o}C for 5 min in an N_2 environment. Finally, the fabricated device was encapsulated with a silicon nitride (SiN) thin film layer by plasma-enhanced chemical vapor deposition and subjected to the electrical measurement procedure.

The dark and photocurrent measurements of the OPD were done with a precision semiconductor parameter analyzer (Agilent 4156C) and a micro probing system (K157MP, Kyowa Riken, Japan) at room temperature. A commercially available RGB LED (HV-5RGB25, Inolux) was used as the light source to illuminate the OPD while doing the measurement. The OPD was illuminated with three different wavelengths red (λ = 624 nm), green (λ = 525 nm), and blue (λ = 470 nm mm)for the photocurrent measurement with supply current controlled irradiation intensity. The luminous intensities of red, green, and blue LEDs were calculated from the illuminance measured by the light meter (AS ONE LM-332) and the distance between the LED and the light meter. The schematic for the measurement system and the actual measurement setup are shown in the following Figure 1.

 doi:10.20944/preprints202408.0609.v1

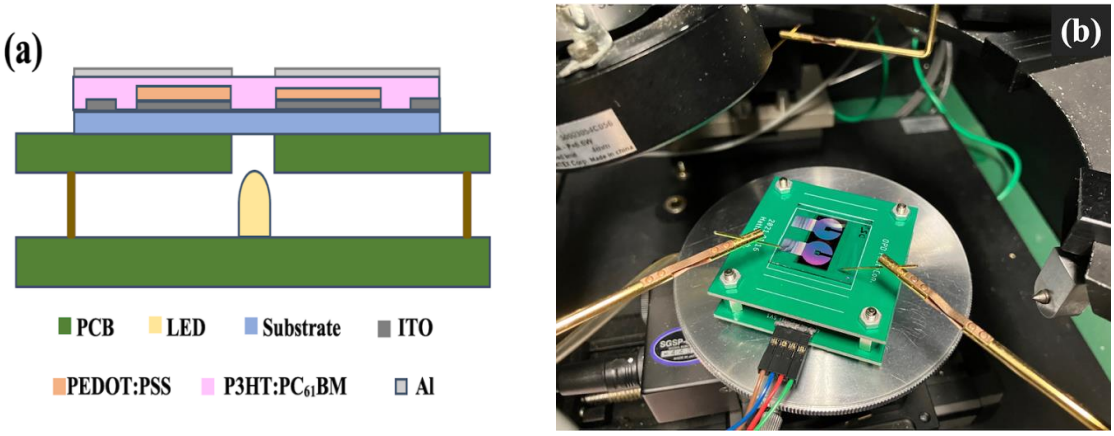

Figure 1. (a) Schematic of *J–V* measurement setup for the OPD. (b) actual image of the parameter analyzer and micro-probing system.

3. Results and discussions

The layer stacks of the device, the chemical structures of the donor and acceptor materials, and the energy diagram of the OPD layer materials are shown in Figure 2. The hole transport layer PEDOT:PSS can support efficient carrier injection and charge collection at the electrode terminal [17]. A typical P3HT:$PC_{61}BM$ blend was adopted for the active layer because it has been extensively used for organic photovoltaic devices even though the power conversion efficiency is limited by a biomolecular recombination loss [18]. Followed by an aluminum top contact, the SiN encapsulation layer was used to protect the device from environmental degradation.

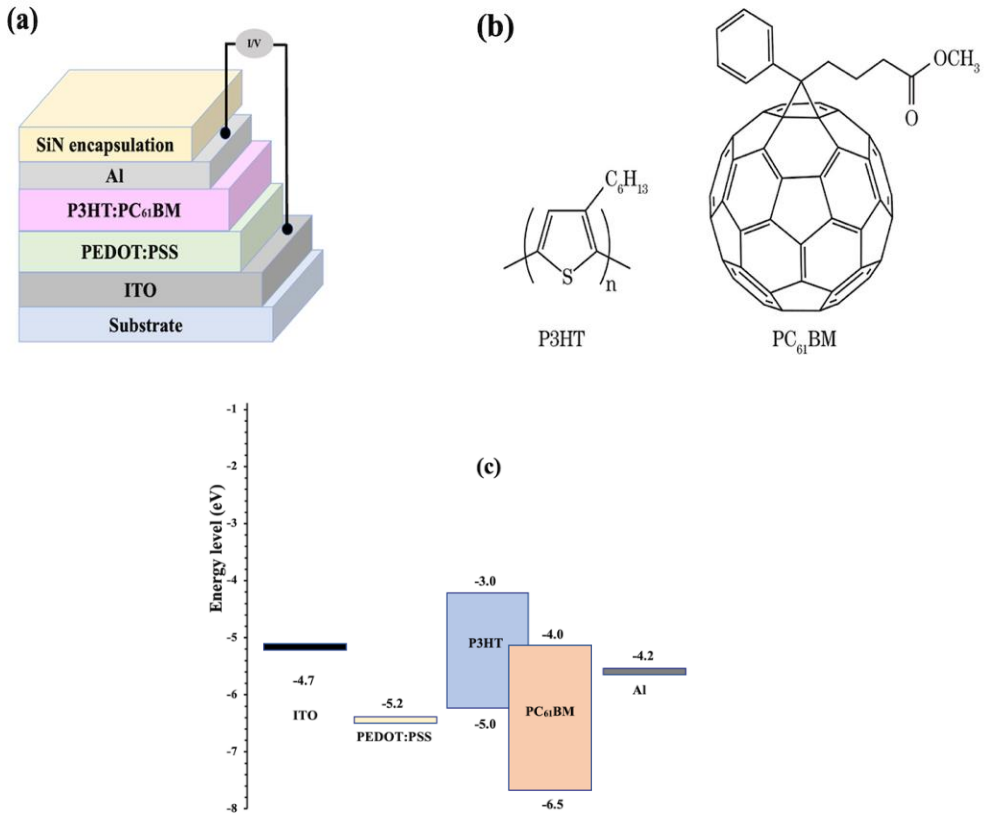

Figure 2. (a) Schematic of OPD device structure. (b) chemical structures of P3HT and $PC_{61}BM$. (c) energy level diagram of OPD layers.

 doi:10.20944/preprints202408.0609.v1

3.1. Effect of LED wavelength on OPD J–V characteristics

Figure 3 shows the schematic of the OPD device (D1) structure and the image of the actual device and the current density-voltage (*J–V*) characteristics both in dark and illumination conditions. The device was illuminated with green, red, and blue light from the rear side as shown in Figure 1. The three LED lights have wavelengths of 470 nm (λ_{blue}), 525 nm (λ_{green}), and 632 nm (λ_{red}) where $\lambda_{blue}<\lambda_{green}<\lambda_{red}$. The photocurrent densities in the OPD, *J–V* characteristics are affected by the illumination of different LED colors which can be observed in Figure 3.

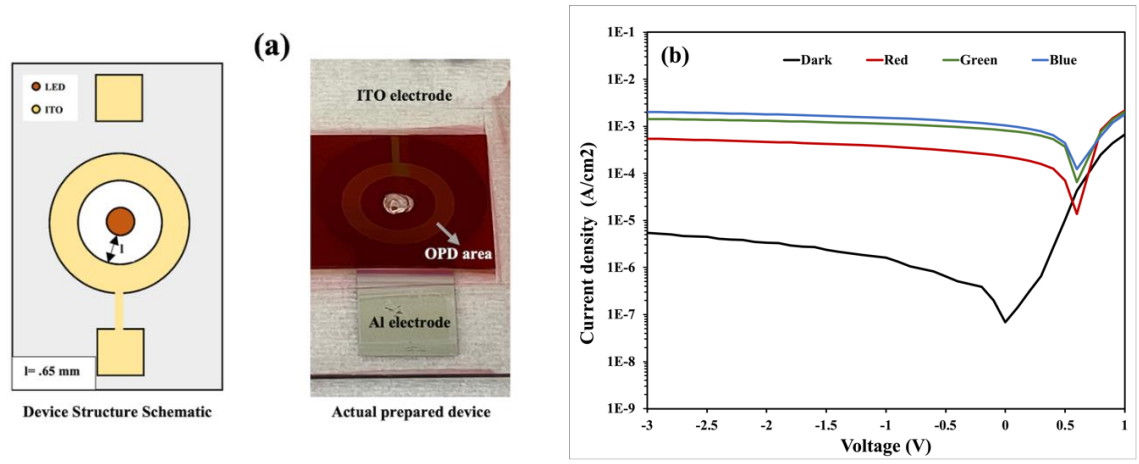

Figure 3. (a) Schematic of the structure and actual image of the fabricated D1 device. (b) the *J-V* characteristics of the D1 device.

The dark current density depends, e.g., on the degree of minority carrier injections such as the electron injection from the PEDOT:PSS layer to the lowest unoccupied molecular orbital (LUMO) of P3HT or $PC_{61}BM$ and the hole injection from Al cathode to the highest occupied molecular orbital (HOMO) of the P3HT or $PC_{61}BM$ [16]. The dark current density and photocurrent density for different LED color illumination at different reverse bias voltages are summarized in Table 1. Under illumination, the OPD photocurrent density shows up to 3–4 orders of magnitude higher than the dark current density at zero bias condition whereas it reduces to 2.5–3 orders of magnitude higher than the dark current at -1 V reverse bias for red, green, and blue incident lights.

Table 1. Current density of D1 device at different illumination conditions.

Illumination condition	**Current density (A/cm²)**				
	-3V	**-2V**	**-1V**	**0V**	**1V**
Dark	5.43E-6	3.35E-6	1.60E-6	6.93E-8	6.78E-4
Red	5.46E-4	4.70E-4	3.75E-4	2.27E-4	2.19E-3
Green	1.43E-3	1.31E-3	1.13E-3	8.17E-4	2.06E-3
Blue	2.03E-3	1.81E-3	1.51E-3	1.04E-3	1.80E-3

In many studies, it has been found that for P3HT:$PC_{61}BM$ heterostructure, the electron donor P3HT has large absorption in a visible wavelength region (380–660 nm) whereas the electron acceptor $PC_{61}BM$ absorbs light in a UV wavelength region (280–380 nm) and their blended structure results in an absorption peak around 470–480 nm [19-21]. Due to the shoulder of the characteristic absorption bands, photons incident on the OPD from LED with a wavelength 470 nm (λ_{blue}) can efficiently generate excitons both in P3HT and $PC_{61}BM$, whereas, photons incident from green and red LED (λ_{green} and λ_{red} respectively) can mainly produce excitons in P3HT acceptor only. The illumination of shorter wavelengths (λ_{blue}) can thus contribute to a larger number of CT exciton generation causing a higher photocurrent density compared to that of the longer wavelengths (λ_{green} and λ_{red}). The relation of the current versus wavelength for the prepared P3HT:$PC_{61}BM$ heterostructure in Figure 4 shows a

 doi:10.20944/preprints202408.0609.v1

higher current value near 470 nm corresponding to λ_{blue}, and it degrades gradually for longer wavelengths corresponding to λ_{green} and λ_{red}.

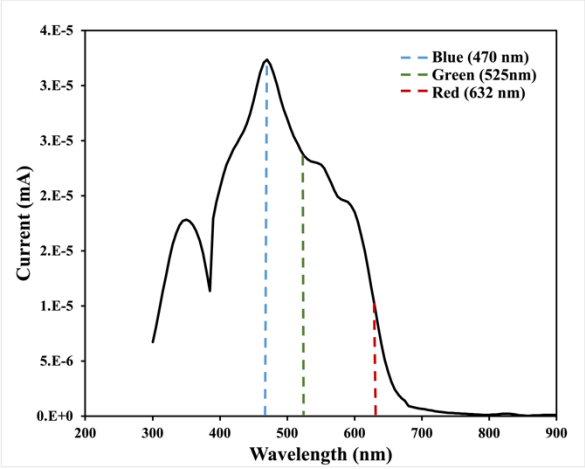

Figure 4. Photocurrent versus incident wavelength for the prepared P3HT:$PC_{61}BM$ OPD device.

3.2. Effect of LED intensity and OPD biasing

For any sensing application, the OPD needs to exhibit a stable and persistent performance over a wide range of light intensity. In this section, we discuss the performance of the OPD for increasing LED luminous intensity under different biasing conditions. The OPD photocurrent density, J_{ph}, highly depends on the intensity of the incident LED illumination. The magnitude of J_{ph} for a particular excitation wavelength, λ, and the light intensity, I_L, can be described by

$$|J_{ph}| = EQE \times \frac{q\lambda}{hc} I_L, \quad (1)$$

where, *EQE* is the external quantum efficiency, h Planck constant, c the light speed and q the elementary charge. The *EQE* depends on the absorption of photons, generation of excitons to be converted into free charge carriers, and collection of carriers before recombination. Equation (1) indicates a proportional dependence of the photocurrent density on the light intensity as far as the *EQE* is unchanged. With increasing light intensity, the number of incident photons and thus the number of photogenerated carriers increases, which in turn increases the J_{ph} [22, 23]. Figure 5 shows the variation of our OPD photocurrent densities, J_{ph} Red, J_{ph} Green and J_{ph} Blue with the LED wavelengths λ_{red}, λ_{green}, and λ_{blue}, respectively, for different OPD biasing voltages with increasing LED luminous intensities, I_L. As a trend, the OPD photocurrent densities are roughly correlated with the incident light intensities linearly. However, a nonlinearity is observed as the light intensities are widely varied. A possible explanation of the deviation from the linearity is a decrease in the *EQE* due to the biomolecular recombination losses for an increasing charge carrier density [16,18]. Another reason for the deviation is that our LED is a point light source, so it is not perpendicularly incident on the OPD surface, while the luminous intensities in Figure 5 have been calculated assuming a planer light source, i.e., the photon numbers incident on the OPD is assumed to be uniform over the area. We will discuss the impact of the light path in Section 3.3.

 doi:10.20944/preprints202408.0609.v1

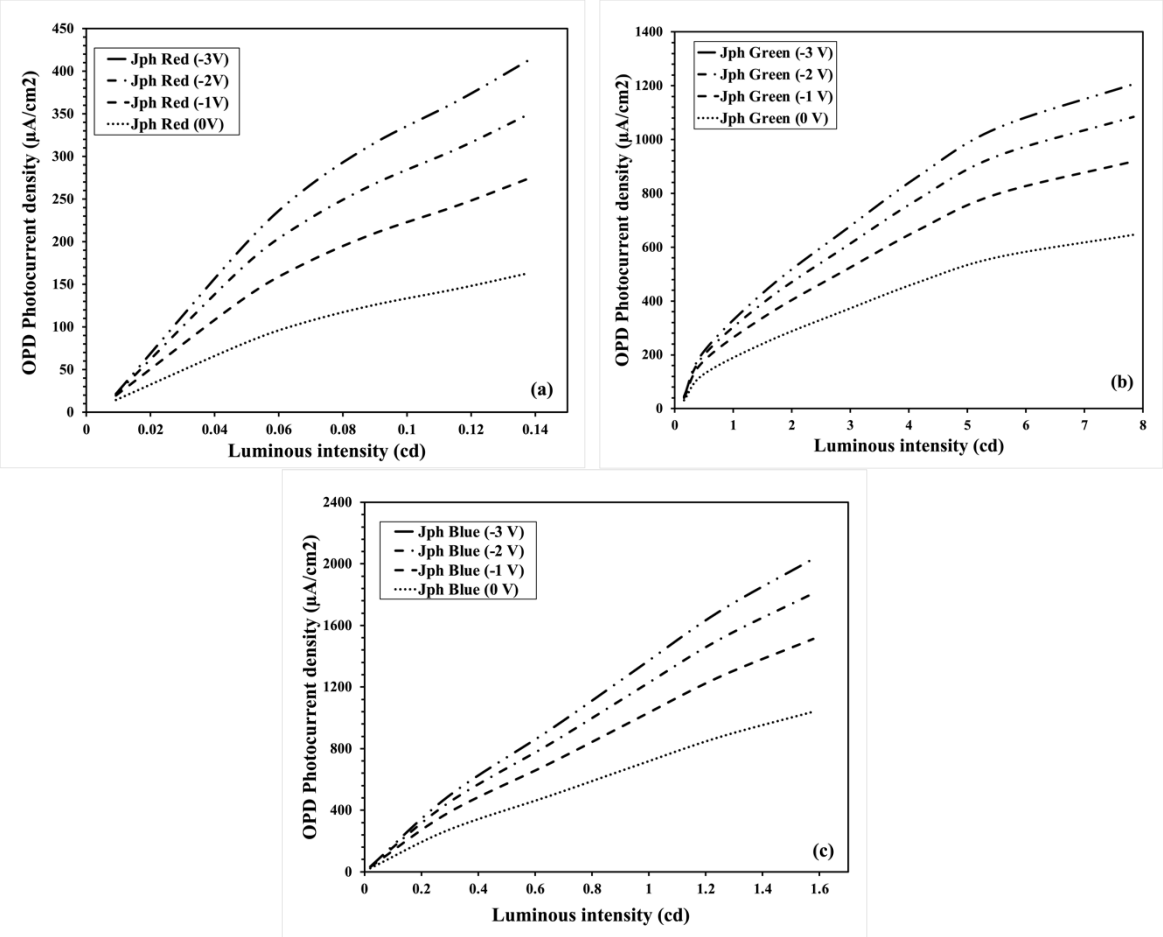

Figure 5. OPD photocurrent density vs LED luminous intensity curves with applied reverse bias condition for (a) red LED, (b) green LED, and (c) blue LED.

A reverse bias voltage in general enhances the strength of the electric field at the junction of photodetector devices as it expedites the carriers' drift velocity and reduces carriers' transit time, enhancing the charge collection and lowering the probability of carrier recombination losses [24]. The transit time, which is inversely proportional to the electric field, can be defined by

$$\tau_t = \frac{l^2}{\mu V}, \tag{2}$$

where V is the bias voltage, l is the space charge layer length at the junction of a conventional photodetector, and μ is the carrier mobility [25]. Although the conventional semiconductor theory is not fully applicable to organic bulk heterojunction devices, the effect of an external field on the carrier collection and the reduction in biomolecular recombination is analogous. Moreover, the dissociation of CT excitons coupled with a coulombic force requires an external field [26]. Due to the combined effects of field dependency, the magnitude of OPD photocurrent I_p increases with the reverse bias applied which can be observed in Figure 4 where the OPD photocurrent magnitude increases for higher reverse bias (-1V to -3V) for LED with red, green, and blue colors.

3.3. Effect of OPD design

In this section, we discuss the OPD performance for different design variations. In sensing applications, designing the OPD plays an important role for the sensors to perform efficiently. The sensor performance depends on the shape of the OPD surface close to the LED, the distance from the LED to the OPD, and the area of the OPD area. The *J–V* characteristics and the on/off ratio of the OPD (ratio of photocurrent to dark current) are also critical parameters. Table 2 shows the design configuration summary of each device used in this study.

Preprints.org (www.preprints.org) | NOT PEER-REVIEWED | Posted: 8 August 2024 doi:10.20944/preprints202408.0609.v1

Table 2. Device configuration summary.

Device label	Area (mm²)	Inner periphery geometry	LED to OPD inner periphery distance, (*l*) (mm)
D1	16	Round	0.65
D2	16	Rectangular	0.65
D3	16	No inner shape	0
D4	16	Round	1.15
D5	32	Round	0.65

3.1. OPD Inner Periphery Shape

Khan *et.al.* showed different sensor geometries (OPD shapes) used for PPG signal analysis [27]. In this work, we used two different geometries of the inner periphery of the OPD active area which is closer to the LED. As shown in Figure 3, device D1 has a circular inner periphery OPD area whereas D2 has a rectangular inner geometry (see Figure 6). Most of the commercial LEDs used in any system have a rectangular shape rather than a dome shape. In the case of rectangular LED, the rectangular inner periphery of the OPD area is convenient as it can collect the LED light from all directions from equal distances. In contrast, for the dome-shaped LED, a circular OPD inner geometry is preferable from the same context. The schematic of the structure, image of the fabricated D2 device, the D2 *J–V* characteristics, and graphs of the on/off ratio for both D1 and D2 devices are shown in Figure 6.

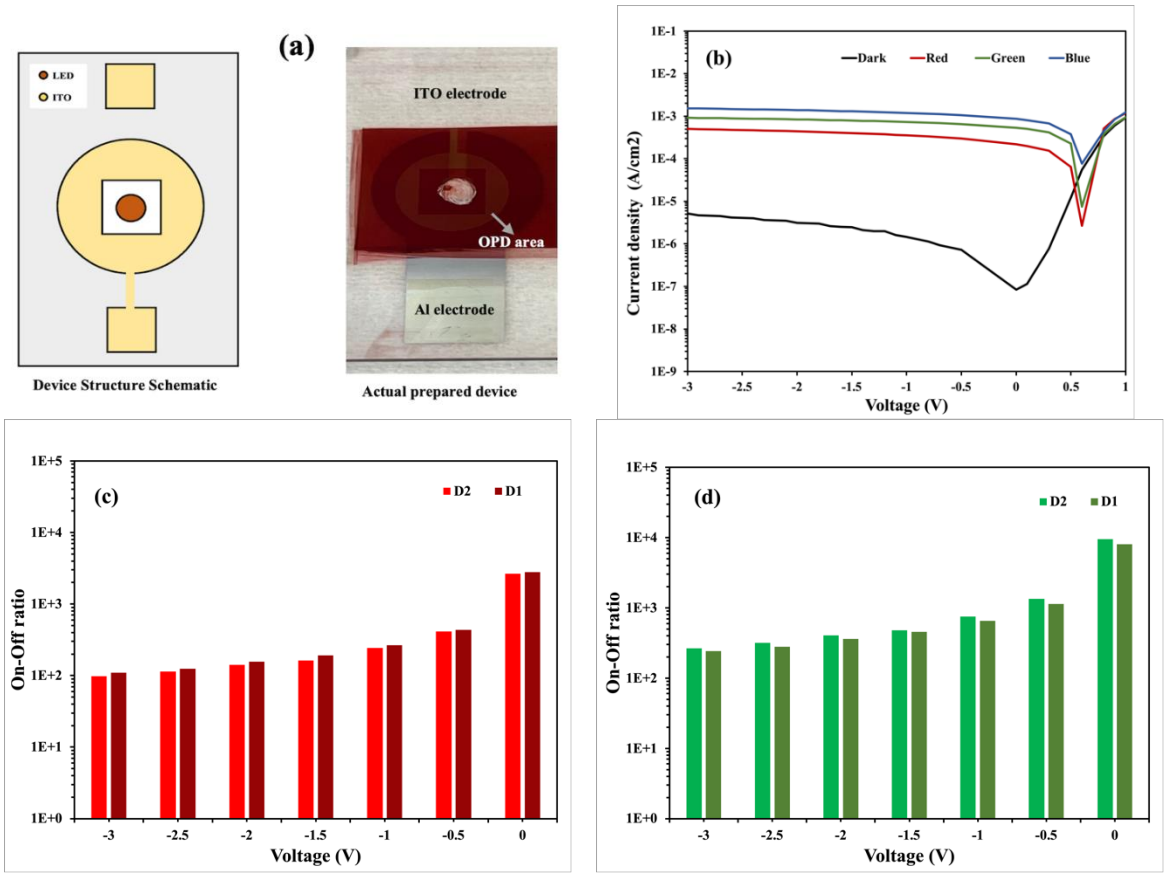

 doi:10.20944/preprints202408.0609.v1

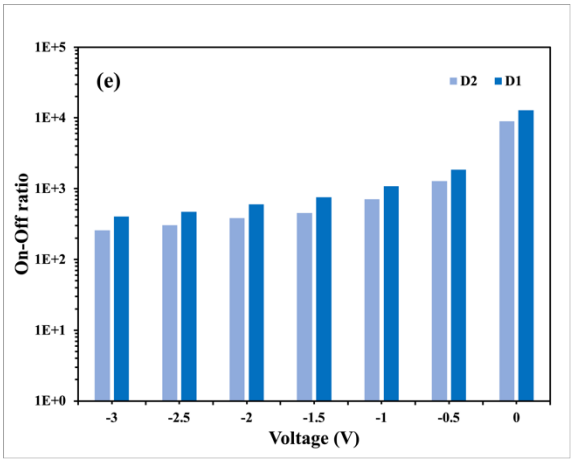

Figure 6. (a) Schematic of the structure and the image of fabricated D2 device. (b) *J–V* characteristics of the D2 device. (c–e) Comparison of the on/off ratio between D1 and D2 devices for red, green, and blue, respectively, LED illumination.

3.3.2. Distance from LED to OPD

Distance from LED and OPD is also an important factor to be considered. Affiq *et. al.* suggested that the light source to detector distance in a reflectance PPG sensor should be kept less than 3mm for efficient signal detection [28]. Here, we have investigated three devices varying the distance from the LED to the OPD. Devices D3, D1, and D4 have distances (*l*), of 0 mm, 0.65 mm, and 1.15 mm, respectively, from the LED surface to the inner periphery of the OPD. The *J-V* curve of device D1 is shown in Figure 3 whereas the schematics of the structures and the *J-V* characteristics of D3 and D4 devices are shown in Figure 7. The dark and photocurrent of these three devices at zero bias conditions (0 V) are summarized in Table 3.

Table 3. Current density of OPD device for varying LED to OPD distance at different illumination conditions.

LED to OPD distance, (*l*) (mm)	**Current density (A/cm²)**			
	Dark	**Red**	**Blue**	**Green**
0 (device D3)	1.12E-8	2.81E-4	1.95E-3	9.75E-4
0.65(device D1)	6.93E-8	2.27E-4	1.04E-3	8.17E-4
1.15(device D4)	7.13E-8	2.12E-4	9.75E-4	7.95E-4

The dark current increases with the increase in OPD to LED distance whereas the photocurrent decreases with increasing the distance. According to the theoretical inverse-square law of radiation, the measured intensity of light is inversely proportional to the source-to-detector distance squared, (l^2) [29]. As the distance from LED to OPD increases, it reduces the number of photons absorbed by the OPD bulk heterojunction materials while it increases the possibility of noise associated with light scattering which in turn reduces the photocurrent and increases the dark current.

 doi:10.20944/preprints202408.0609.v1

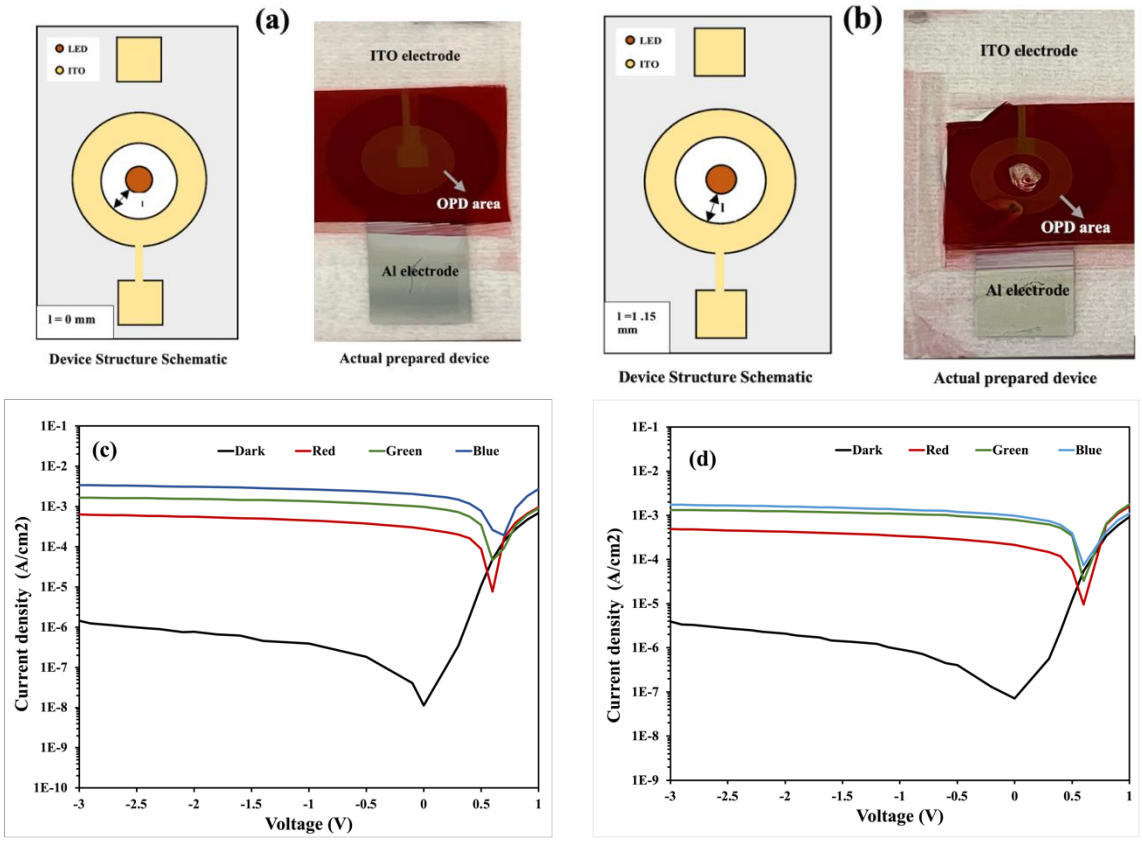

Figure 7. (a, b) Schematics of the structures and the image of fabricated devices D3 (*l*= 0mm), and D4 (*l*= 1.15mm), respectively (c, d) the *J–V* characteristics of devices D3 and D4, respectively.

The graphs of the on/off ratio comparison between D1, D3, and D4 devices are shown in Figure 8 for red, green, and blue incident illumination. A decreasing trend of the on/off ratio is observed when the source-to-detector distance *(l)* (D3> D1>D4) is increased. As summarized in Table 3, the trend of the on-off ratio is the consequence of the reducing photocurrent and the increasing dark current with increasing *l*.

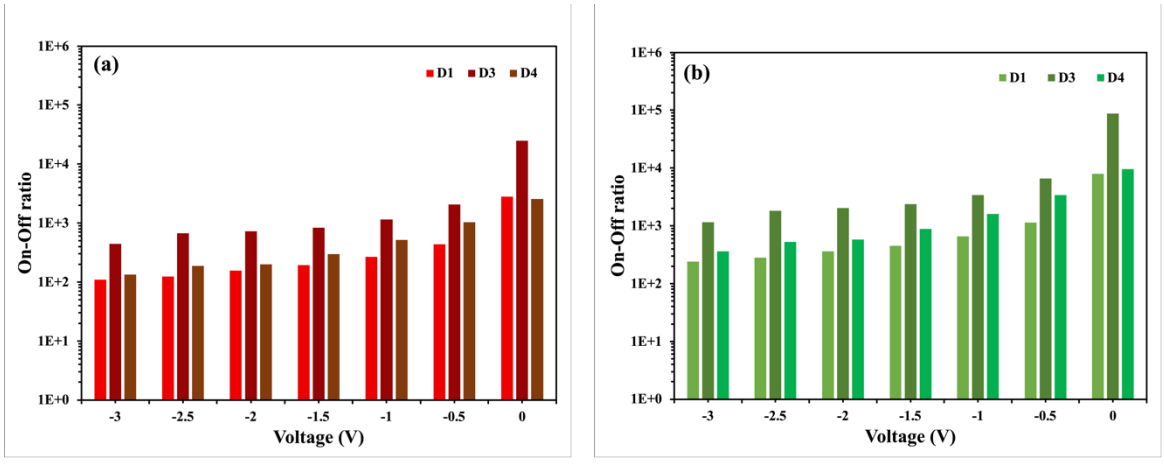

Preprints.org (www.preprints.org) | NOT PEER-REVIEWED | Posted: 8 August 2024 doi:10.20944/preprints202408.0609.v1

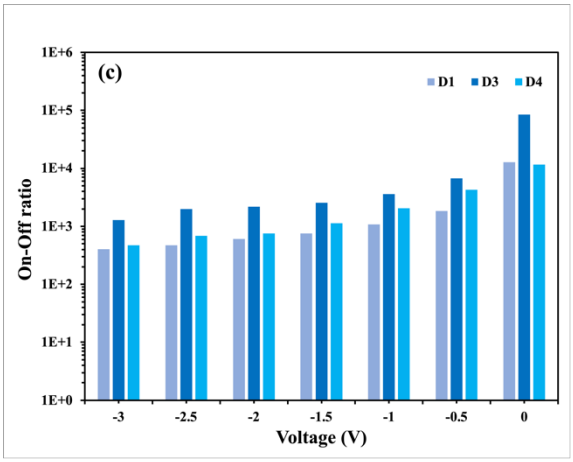

Figure 8. (a–c) Comparison of on/off ratio between D1(*l*= 0.65mm), D3 (*l*= 0mm), and D4 (*l*= 1.15mm) devices for red, green, and blue, respectively, LED illumination.

3.3.3. OPD area

One of the advantages of organic photodetector is that it can be fabricated over a large area. OPD's area can affect its dark and photocurrent density. We investigated the effect of the area size by comparing two OPD devices with active areas of 16 mm² (D1) and 32 mm² (D5) with the same inner periphery and distance from the incident LED (*l* = 0.65 mm). The *J*–*V* curve of device D5 and graphs of the on-off ratio comparison between devices D1 and D5 are shown in Figure 9.

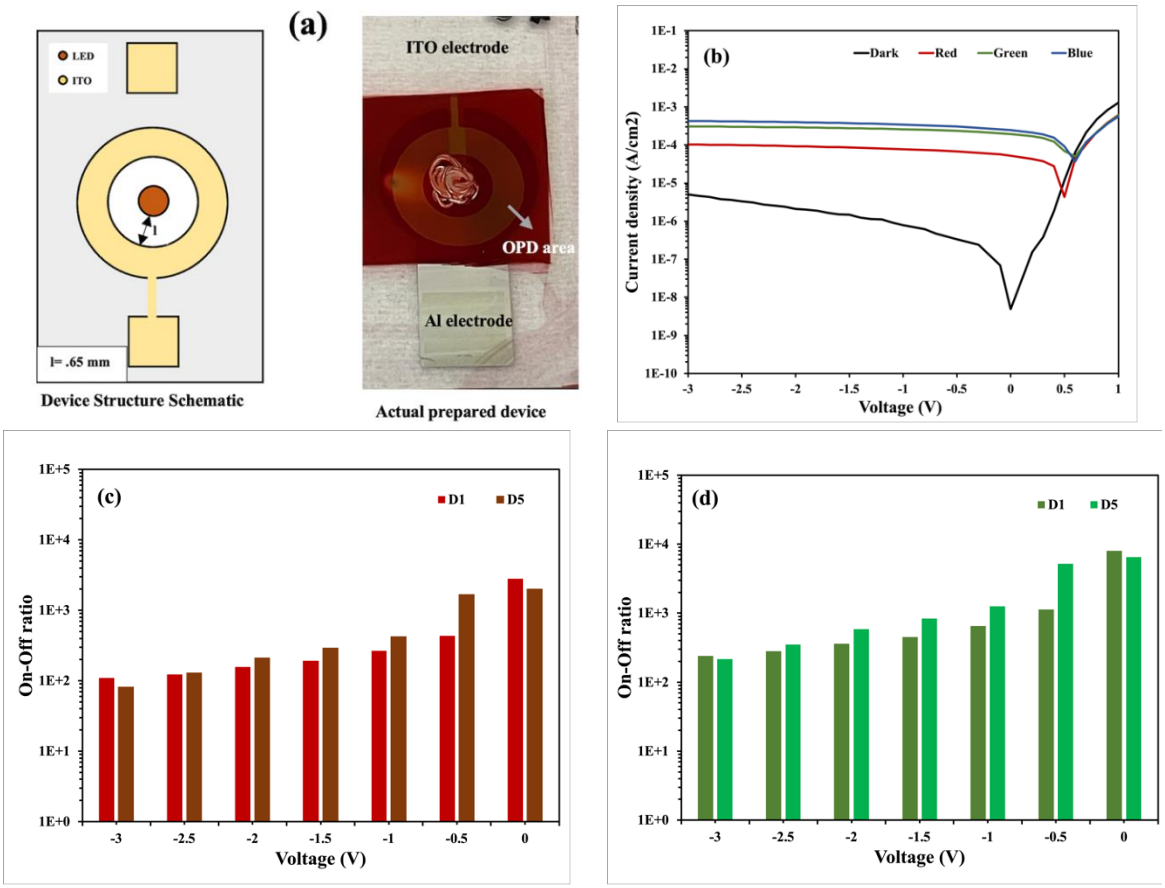

 doi:10.20944/preprints202408.0609.v1

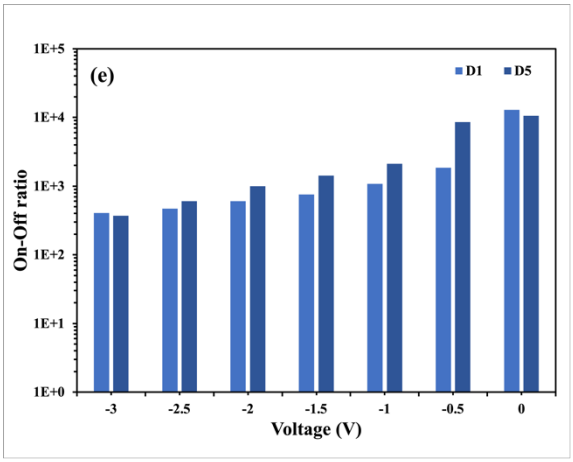

Figure 9. (a) Schematic of the structure and the image of fabricated D5 device. (b) *J–V* characteristics of the D5 device, (c–e) Comparison of on/off ratio between D1 and D5 devices for red, green, and blue, respectively, LED illumination.

Increasing the active area allows more photons to be absorbed in the OPD and contributes to a larger number of charge carrier generation in total. If the LED incident is normal to the OPD active area and light intensity is uniform over the area, the value of the photocurrent density does not depend on the area according to the definition (A/cm^2). In our OPD-LED hybrid system, the LED is a point source, i.e., the light spreads radially and it follows a path through reflection to reach the OPD active area (see Figure 1). Therefore, a larger OPD area has some disadvantages in uniform light illumination. In addition, it has been known that an increase in the area can enhance the probability of having defects that accelerate electron and hole recombination at low built-in junction potential and thus, the photocurrent density in organic bulk heterojunction is often area size dependent [30]. The above two factors should be the reason behind the lower photocurrent density of device D5 seen in Figure 9b compared to the other devices. The inferior zero bias on/off ratio of D5 compared to that of D1 seen in Figure 9c-e can be attributed to the lower photocurrent density in D5. However, as we discussed earlier, applying a reverse bias voltage decreases the probability of carrier recombination losses. This explains the superior on-off ratio of the D5 device at reverse bias conditions. However, At the highest reverse bias (-3 V), the on-off ratio of D5 is lowered again due to the increasing dark current possibly associated with minority carrier injections.

4. Conclusion

In this work, we have demonstrated the performance of an OPD-LED hybrid system, i.e., a combination of an OPD and an incident LED. The role of LED forward current and different OPD biasing conditions was studied. The results indicated a higher magnitude of OPD photocurrent at higher reverse bias conditions due to enhanced charge carrier generation and collection. The OPD *J–V* characteristics were investigated for different LED lights having different wavelengths and a higher current density was observed for shorter incident wavelength, i.e., for blue LED. We have further investigated the OPD *J–V* characteristics and the on/off ratio for different shapes of the OPD inner periphery, different distances between the OPD and the incident LED, and different sizes of the OPD area. The obtained results suggested that the distance between LED and OPD should be minimized to obtain a low dark current and a high photocurrent, i.e., a high on/off ratio suitable for any kind of sensing application. The variation for the OPD area suggested that the OPD area should be larger if the OPD is used at zero bias condition whereas OPD should possess a smaller area if it is used at a reverse bias condition. The observations presented in this paper can be of great importance for optimizing OPD structure and OPD operating conditions for different sensing applications.

Author Contributions: Conceptualization, R.H., F.A.J, M.A.B.M; methodology, all authors; software, M.A.B.M; validation, R. H.; writing—original draft preparation, F.A.J.; writing—review and editing, R.H., F.A.J., K.H.; supervision, R.H. All authors have read and agreed to the published version of the manuscript.

Funding: This research received no external funding.

Data Availability Statement: Data are contained within this article.

Acknowledgments: The continuous support from Kyushu University, the Ministry of Education, Culture, Sports, Science and Technology (MEXT), Japan, and the Japan International Cooperation Agency (JICA) is highly appreciated.

Conflicts of Interest: The authors declare no conflicts of interest

References

1. T. Sekitani, T. Someya, Stretchable, Large-area Organic Electronics, *Adv. Mater*. **2010**, 22, 2228−2246.
2. R. Nie, Y. Wang, X. Deng, Aligned Nanofibers as an Interfacial Layer for Achieving High-Detectivity and Fast-Response Organic Photodetectors, *ACS Appl. Mater. Interfaces.* **2014**, 6, 7032−7037
3. R. D. Jansen-van Vuuren, A. Armin, A. K. Pandey, P. L. Burn, P. Meredith, Organic Photodiodes: The Future of Full Color Detection and Image Sensing, *Adv. Mater*. **2016**, 28, 4766−4802
4. Y. S. Rim, S.-H. Bae, H. Chen, N. De Marco, Y. Yang, Recent Progress in Materials and Devices toward Printable and Flexible Sensor, *Adv. Mater*. **2016**, 28, 4415−4440
5. K.-J. Baeg, M. Binda, D. Natali, M. Caironi, Y.-Y. Noh, Organic Light Detectors: Photodiodes and Phototransistors, *Adv.Mater*. **2013** ,25, 4267−4295
6. G. Simone, D. Di. C. Rasi, X. de Vries, G. H. L. Heintges, S. C. J. Meskers, R. A. J. Janssen, G. H. Gelinck, Near-Infrared Tandem Organic Photodiodes for Future Application in Artificial Retinal Implants, *Adv. Mater*. **2018**, 30, 1804678
7. G. Simone, M. J. Dyson, S. C. J. Meskers, R. A. J. Janssen, G. H. Gelinck, Organic Photodetectors and their Application in Large Area and Flexible Image Sensors: The Role of Dark Current, *Adv. Funct. Mater*. **2020,** 30, 1904205
8. Y. Khan, A. E. Ostfeld, C. M. Lochner, A. Pierre, A. C. Arias, Monitoring of Vital Signs with Flexible and Wearable Medical Devices. *Adv. Mater*. **2016**, 28, 4373-4395.
9. J. Clark, G. Lanzani, Organic photonics for communications. *Nat. Photonics*. 2010, 4, 438– 446
10. H. Lee, E. Kim, Y. Lee, H. Kim, J. Lee, M. Kim, H. J. Yoo, S. Yoo, Toward all-day wearable health monitoring: An ultralow-power, reflective organic pulse oximetry sensing patch, *Sci. Adv.* **2018**, 4, eaas9530.
11. P. Zalar, N. Matsuhisa, T. Suzuki, S. Enomoto, M. Koizumi, T. Yokota, M. Sekino, T. Someya, A Monolithically Processed Rectifying Pixel for High-Resolution Organic Imagers, *Adv. Electron. Mater*. **2018**, 4, 1700601
12. X. Gong, M. Tong, Y. Xia, W. Cai, J. S. Moon, Y. Cao, G. Yu, C-L. Shieh, B. Nilsson, A. J. Heeger, High-detectivity polymer photodetectors with spectral response from 300 nm to 1450 nm. *Science.* **2009**, 325, 1665-1667
13. E.-C. Chen, C.-Y. Chang, J.-T. Shieh, S.-R. Tseng, H.-F. Meng, C.-S. Hsu, S.-F. Horng, Polymer photodetector with voltage-adjustable photocurrent spectrum, *Appl. Phys. Lett.* **2010**, 96, 043507
14. P. E. Keivanidis, P. K. H. Ho, R. H. Friend, Greenham, The Dependence of Device Dark Current on the Active-Layer Morphology of Solution-Processed Organic Photodetectors, *Adv. Funct. Mater*. **2010**, 20, 3895– 3903
15. X. Liu, H. Wang, T. Yang, W. Zhang, X. Gong, Solution-Processed Ultrasensitive Polymer Photodetectors with High External Quantum Efficiency and Detectivity, *ACS Applied Materials & Interfaces*. **2012**, 4, 3701-3705
16. S. Shafian, Y. Jang, K. Kim, Solution processed organic photodetector utilizing an interdiffused polymer/fullerene bilayer, *Opt. Express*. **2015**, 23, A936-A946
17. P. Saha, P. Karmakar, D. Deb, Modeling and simulation of P3HT and PCBM based organic optoelectronics devices, *Materials Today: Proceedings*, **2021**, 43, 3438-3442
18. C.G. Shuttle, R. Hamilton, J. Nelson, B.C. O'Regan, J.R. Durrant, Measurement of Charge-Density Dependence of Carrier Mobility in an Organic Semiconductor Blend, *Adv. Funct. Mater*., **2010**, 20, 698-702
19. J. Mullerova, M. Kaiser, V. Nadazdy, P. Siffalovic, E. Majkova, Optical absorption study of P3HT:PCBM blend photo-oxidation for bulk heterojunction solar cells, *Sol. Energy*, **2016**, 134, 294-301
20. Y. A. M. Ismail, T. Soga, T. Jimbo, Effect of composition on conjugation structure and energy gap of P3HT:PCBM organic solar cell, *Int. J. New. Hor. Phys*., **2015**, 2, 87-93
21. Y. Xin, Z. Wang, L. Xu, X. Xu, Y. Liu, F. Zhang, UV-Ozone treatment on CS_2CO_3 interfacial layer for the improvement of inverted solar cell, J. Nanomater., **2013**, 104825
22. S. Zeiske, W. Li, P. Meredith, A. Armin, O. J. Sandberg, Light intensity dependence of the photocurrent in organic photovoltaic devices, *Cell Rep. Phys. Sci.*, **2022**, 3, 101096.
23. A. Mahapatra, V. Anilkumar, R. D. Chavan, P. Yadav, D. Prochowicz, Understanding the origin of light intensity and temperature dependence of photodetection properties in MAPbBr3 single-crystal-based photodetector, *ACS Photonics*, **2023**, 10, 1424-1433.

 doi:10.20944/preprints202408.0609.v1

24. Q. Lv, F. Yan, X. Wei, K. Wang, High-performance, self-driven photodetector based on graphene sandwiched GaSe/WS2 heterojunction, *Adv. Opt. Mater.*, **2018**, 6, 1700490
25. S. Verma, R. Yadav, A. Pandey, Investigating active area dependent high performing photoresponse through thin films of Weyl Semimetal WTe_2. *Sci Rep*. **2023**, 13, 197
26. H. H. P. Gommans, M. Kemerink, J. K. Kramer, R. A. J. Janssen, Field and temperature dependence of the photocurrent in polymer/fullerene bulk heterojunction solar cells, *Appl. Phys. Lett.*, 2005, 87, 122104
27. Y. Khan, D. Han, J. Ting, M. Ahmed, R. Nagisetty and A. C. Arias, Organic Multi-Channel Optoelectronic Sensors for Wearable Health Monitoring, ***IEEE Access***, **2019**, 7, 128114-128124
28. M. A. B. Misran, A. Bilgaiyan, R. Hattori, Optical ray tracing simulation by using Monte Carlo method for reflectance-based photoplethysmography sensor in human skin and fingertip model, *Computational And Experimental Research In Materials And Renewable Energy*, **2022**, 5, 78-91.
29. J. R.S. Brownson, *Solar Energy Conversion Systems*, First edition, Elsevier, Oxford, 2014
30. W. -I. Jeong, J. Lee, J. -J. Kim, Reduction of collection efficiency of charge carriers with increasing cell size in polymer bulk heterojunction solar cells, *Adv. Funct. Mater*., **2011**, 21, 343-347.